Journal of Applied Physics

RESEARCH ARTICLE | JULY 23 2018

# Linear scanning tunneling spectroscopy over a large energy range in black phosphorus

Hongli Guo; Xingxia Cui; Weiqing Zhou; Ding Han; Chungwei Lin; Limin Cao; Min Feng



*J. Appl. Phys.* 124, 045301 (2018)
https://doi.org/10.1063/1.5029571

# Linear scanning tunneling spectroscopy over a large energy range in black phosphorus

Hongli Guo,[1,a)] Xingxia Cui,[1,a)] Weiqing Zhou,[1] Ding Han,[1] Chungwei Lin,[2] Limin Cao,[1] and Min Feng[1,3]
[1]*School of Physics and Technology, Center for Nanoscience and Nanotechnology, and Key Laboratory of Artificial Micro- and Nano-structures of Ministry of Education, Wuhan University, Wuhan 430072, China*
[2]*Mitsubishi Electric Research Laboratories, 201 Broadway, Cambridge, Massachusetts 02139, USA*
[3]*Institute for Advanced Study, Wuhan University, Wuhan 430072, China*

(Received 15 March 2018; accepted 4 July 2018; published online 23 July 2018)

We reveal the unique electronic characteristics of the conduction band (CB) of black phosphorus (BP) by combining low-temperature scanning tunneling microscopy/spectroscopy (STM/STS), density functional theory calculations, analytic fitting, and model simulations. We discover that the differential conductance spectrum, which represents the local density of states (LDOS) of BP, exhibits a linear character over a large energy range in the unoccupied electronic state region. Combining theoretical calculations, we demonstrate that the linear character right above the conduction band minimum originates from a specific combination of the anisotropic band dispersions of BP's CB. In particular, the wave function of BP's CB possesses a pronounced density between BP layers and extends into the vacuum significantly, which is in sharp contrast to those of adjacent bands. This makes the CB dominate STS signals even when the energy is sufficiently high to involve other bands, and maintains the linearity of the STS spectrum over a wide energy range. The fact that the CB provides linear DOS and possesses pronounced wave function density in BP interlayers provides new insights for engineering the electronic structures and properties of BP and BP based materials. *Published by AIP Publishing.* https://doi.org/10.1063/1.5029571



## I. INTRODUCTION

Black phosphorus (BP) was recently rediscovered from the perspective of layered semiconductors for promising applications in nanoelectronics and nanophotonics,[1–9] with its tunable band-gap,[10–13] high carrier mobility,[1–6,14] and intrinsic in-plane anisotropy.[1–6,14,15] In addition, it has been proposed that the band structures of BP can be manipulated by strain, electric fields, or surface doping to induce a superconducting phase transition,[16] a metal-insulator transition,[17] and a semiconductor to semimetal transition.[18] The variety of displayed phases makes the BP based materials attractive for both fundamental research and practical applications. However, there are only limited experimental reports on the intrinsic electronic structure of BP surface. Within these reports, the electronic structure of BP is only probed in the energy range around the valence band maximum (VBM) and conduction band minimum (CBM), leaving a detailed understanding of its electronic characteristics deficient.[19–23]

In this work, we study the local electronic properties of bulk BP surface over an extended energy window. Our experimental results revealed a linear scanning tunneling spectroscopy (STS) spectrum over a wide energy range from CBM to 1.41 eV above. Linear-shaped STS normally occurs in certain 2D materials at a small energy range,[24–29] but is rarely observed in 3D materials. In addition, the linear character of the local density of states (LDOS) over an energy window of 1.4 eV has never been reported in other materials. By utilizing DFT calculations and analytic fitting, we conclude that the particular dispersion of the CB band of bulk BP, linear in the armchair direction but parabolic in the zigzag and interlayer directions, gives rise to the linearity close to CBM. For the monotonous linearity of STS spectra extending into the energy window well above CBM, we argue that another characteristic of CB, its quite delocalized wave function density within BP interlayers, plays an important role. These findings offer new insights into BP's electronic band structure and can be useful for engineering the electronic and optical properties of BP and the related materials.

## II. METHODS

### A. Experiments

The experiments were carried out in an ultrahigh vacuum low temperature scanning tunneling microscopy (STM) system (CreaTec). The BP crystals were home-grown using a chemical vapor transport (CVT) method in a two-zone tube furnace with red phosphorus, tin iodide ($SnI_4$), and tin powders as the starting materials. For STM experiments, BP bulk crystals were cleaved *in-situ* in preparation chamber under ultrahigh vacuum at room temperature (RT). The sample with freshly cleaved surface was then immediately transferred into the STM chamber, and cooled down to 77 K and/or 5.0 K. STM images were acquired in the constant-current mode. STS measurements were performed with a lock-in technique with a bias modulation of 15 mV at 321.333 Hz. The STM tips were chemically etched tungsten or mechanically cut Pt-Ir wires, which were further calibrated spectroscopically against the Shockley surface states of cleaned Cu (111) or Au (111) surfaces before being utilized on BP.

[a)]H. Guo and X. Cui contributed equally to this work.

### B. DFT calculations

First-principle DFT calculations were performed using the Vienna *Ab initio* Simulation Package.[30,31] We use the Perdew-Burke-Ernzerhof (PBE) exchange-correlation functional along with the projector-augmented wave potentials for the self-consistent total energy calculations and geometry optimization.[32–34] The energy cutoff for the plane-wave basis is set to 500 eV for all the calculations. A K-mesh of $40 \times 40 \times 10$ is adopted to sample the first Brillouin zone (BZ) of the conventional unit cell of bulk BP. 60 points are collected along each high symmetry line in the reciprocal space in the band structure calculations. Van der Waals (vdW) interactions are included at the vdW-DF level with the optB88 exchange functional (optB88-vdW) when optimizing the system geometry.[35,36] The unit cell is optimized until all atoms in the cell are allowed to relax to the point that the residual force per atom is 0.01 eV Å$^{-1}$. The calculated lattice constants for bulk BP are $a = 3.348$ Å, $b = 4.587$ Å, and $c = 11.033$ Å, which are in good agreement with experimental values and other theoretical calculations.[2,14,37]

## III. RESULTS AND DISCUSSION

A schematic illustration of the BP structure is shown in Fig. 1(a). Within one atomic BP layer, the P atoms are puckered into two different planes, as shown in the side view at lower left panel in Fig. 1(a). Figure 1(b) shows a STM topography image of BP with atomic resolution. Since the upper atoms sit directly above the lower ones in a puckered layer, it is not possible to image the lower atoms using STM. Normally, the STM image of BP surface is an array of zigzag chains composed only of the upper atoms [Fig. 1(b)]. The experimental observation about the chain lattice constant along the zigzag ($a = 3.3 \pm 0.1$ Å) and armchair ($b = 4.3 \pm 0.1$ Å) directions, and the detailed contrast [P1 for brighter atoms and P2 for darker ones in Fig. 1(b), inset] of the atoms within the chains, are in good agreement with other reports.[19]

Figure 1(c) shows a typical d$I$/d$V$ spectrum obtained on BP surface in the energy range of −2.5 eV to 3.0 eV. Over this wide energy window, we observe a unique character of STS. As seen in Fig. 1(c), after a sharp increase just above the CBM at ∼0.25 eV, the signals increase linearly up to 1.41 eV. Normalizing the d$I$/d$V$ spectrum using the Wentzel-Kramers Brillouin (WKB) approximation does not change the character of the spectrum.[38] For clarity, we add a dashed straight line next to the experimental data to emphasize the almost perfect linearity of the d$I$/d$V$ spectrum. At 1.41 eV, the STS signal starts decreasing and again shows a linear character to form a Λ-shaped peak. We attribute the turning point (peak) at 1.41 eV to a sudden decrease in electron states, which might correspond to a Van Hove Singularity that lies at around 1.5 eV along the Z-T direction as shown in

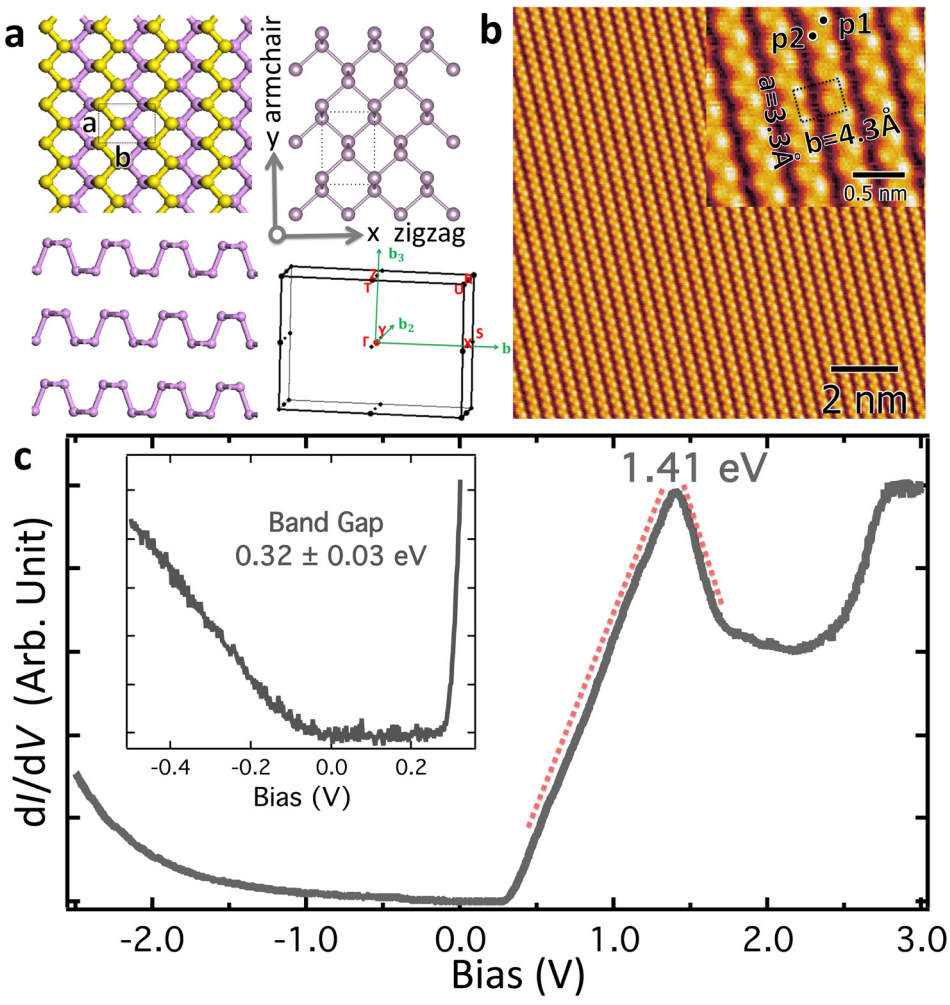


FIG. 1. (a) The model structure and the first surface BZ of BP. (b) Constant-current STM image of BP ($V_S = -0.6$ V, $I_t = 60$ pA). Close-up shows that only the upper atoms of the topmost puckered layer can be seen with no reconstruction. The surface unit cell is indicated by black dashed lines. (c) A typical d$I$/d$V$ spectrum acquired on BP surface in the energy window from −2.5 eV to 3.0 eV. The measured band gap is shown in inset figure.

the band structure below in Fig. 2(a) (marked with the blue-dotted circle). The large range linearity of the STS from BP has never been reported in other materials. To clarify the reliability of the STS data, we have repetitively checked the BP samples by different *in-situ* processed Pt-Ir and tungsten tips. The phenomena are fully repeatable and reproducible. As a linear-shaped STS implies a linear density of states (DOS), we first study the band structures and DOS of BP by DFT calculations.

It is well known that DFT functionals, such as PBE, typically underestimate the band gap. In our calculations, we first check the calculations without taking into account the van der Waals interaction. The calculated gap is only 30 meV in this case, consistent with the previous work.[39] Using PBE + optB88 + vdW functional, the calculations give a direct band gap of 0.20 eV, which is reasonably close to our experimental value of 0.32 eV [Fig. 1(c), inset, and Fig. S1, supplementary material]. Therefore, the DFT calculations provide a reasonable description for the electronic structure of bulk BP. Figures 2(a) and 2(b) show the calculated band structure and DOS of BP. In Fig. 2(a), we see the CBM located at Γ point, which corresponds to the turning point with abrupt intensity increasing in the d$I$/d$V$ measurements [Fig. 1(c)]. In addition, in the energy range from the CBM to ∼0.5 eV there exists only one band, the lowest CB. Above 0.5 eV, more conduction bands appear. As a consequence, the calculated DOS [Fig. 2(b), the numerical integration of the band structure] shows a small shoulder at ∼0.65 eV and a peak at ∼0.9 eV, corresponding to energy locations where new bands start contributing. As several bands are involved in this energy range, a linear DOS and thus a STS profile is not expected. This raises the question about the origin of experimentally observed linear STS spectrum from the CBM to 1.41 eV. Below, we employ DFT calculations and analytic fitting to answer the question. We note that our DFT calculations, as shown in Fig. 2(b), also reveal two peaks at ∼−1.8 eV and +2.3 eV, which are not obvious in the experiments [Fig. 1(c)]. The discrepancy might come from the detection sensitivity as is discussed in supplementary material (Fig. S2).

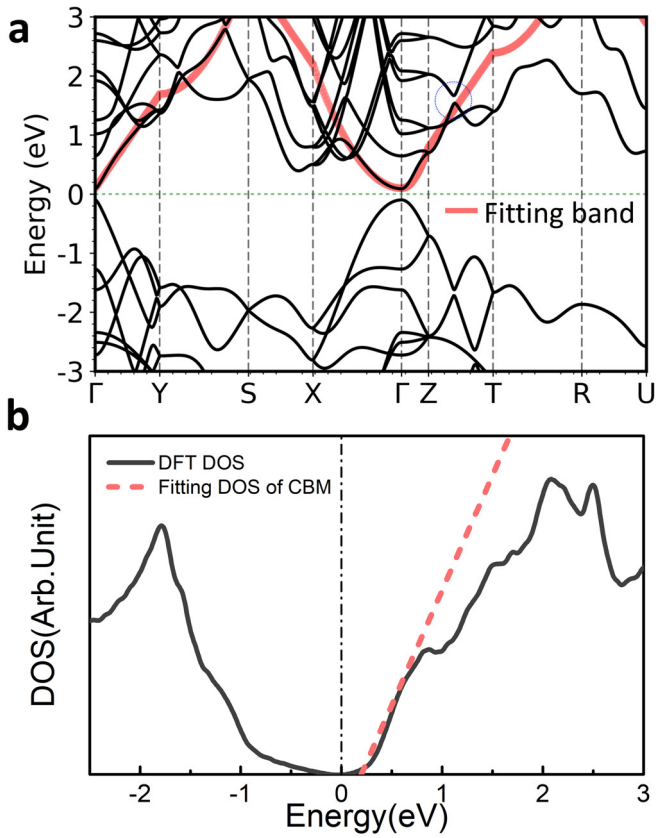


FIG. 2. (a) DFT band structure of bulk BP and the fitting conduction band minimum $[E(k_x, k_y, k_z) = 8.38k_x^2 + 3.19|k_y| + 2.79k_z^2 + 0.1]$. (b) The DOS of bulk BP integrated from the DFT band structure (dark black) and the fitting band (red line) in (a). (The DOS of DFT is obtained using a broadening width of 0.05.)

Despite DFT fails to produce the linear LDOS over the entire 1.4 eV energy window, the calculated DOS does show a linear character from the CBM to ∼0.5 eV, which is consistent with the experimental results. To resolve the physical origin of the linear DOS just above CBM, we first consider the linearly shaped STS in other Dirac-like 2D materials. In graphene, the linear STS near the Fermi energy originates from the linearly dispersing bands, i.e., $E \propto |k|$. The corresponding linear DOS $N(E)$ can be derived from $N(E) \propto |k| \propto E$ and leads to a linear STS spectrum close to Fermi energy. Unlike the isotropic graphene, however, there is an intrinsic in-plane anisotropy in BP. We see in Fig. 2(a) that the CB possesses a very distinct anisotropy—it is linear along the Γ-Y and parabolic along the Γ-X and Γ-Z directions. BP's anisotropic bands and the related anisotropic electronic and optical applications have been explored by a large amount of experimental and theoretical work.[14,18,39–42] In the following, we demonstrate that this band anisotropy is responsible for the experimentally observed linear STS spectrum in BP in the energy region just above CBM.

First, we apply an analytic fitting to simulate the DFT bands and DOS of BP. Here, we only take CB into account in the fitting. Because above 0.5 eV there are more bands involved and a single dispersion becomes insufficient, the fitting could only explain the DOS in the energy range from the CBM to ∼0.5 eV. The red curve in Fig. 2(a) represents the fitting band around Γ-point by utilizing the expression of $E(k_x, k_y, k_z) = 8.38k_x^2 + 3.19|k_y| + 2.79k_z^2 + 0.1$, corresponding to the linear dispersed band along Γ-Y and the parabolic bands along Γ-X and Γ-Z. It can be seen that the fitted band agrees with the DFT band pretty well. During the fitting, we simplify the problem by ignoring the cross term such as $|k_xk_y|$ and confirm the validity of the fitting dispersion by checking the fitting band and DFT band along Γ − $S$ (0.5, 0.5, 0). (see Fig. S3 in supplementary material). We further confirm that the dispersion of the form $E(k) = ak_x^2 + b|k_y| + ck_z^2 + d$ leads strictly to a linear DOS with $(E) \propto \frac{V}{4\Pi^3}\frac{4}{b\sqrt{ac}}(E-d)$, as plotted in Fig. 2(b). In the supplementary material, the origin of the anisotropic band dispersion in BP (Fig. S4, supplementary material) is discussed. The results show that for the quasi "3D" system, all $k_x$, $k_y$, $k_z$ dependences (one linear and two parabolic) of the band dispersion are important in producing the linear LDOS. We need to mention that due to the smoothness of the dispersion, the existence of a strictly linear-dispersed band at the band edge

cannot be exact (as its derivative is not continuous); thus, the linear fitting can only be treated as an approximation to the band dispersion.

After explaining the physical origin of the linear shaped STS in the energy range just above CBM, we now explore why the STS spectrum also shows the linear profile well above 0.5 eV, where more CB bands contribute the d$I$/d$V$ signals.

In the experiments, when performing the constant-current scanning, we noticed that changing the tunneling from occupied states to unoccupied states is always accompanied with a pronounced tip retraction of about 1.5–2.0 Å, and vice versa. This significant change in tip-height implies one to two orders' tunneling conductance difference between the occupied states and the unoccupied states if the tip height is kept constant. In addition, the STS spectra always show much smaller signal intensity from the occupied states compared with those from the unoccupied states with the similar bias range. For example, the d$I$/d$V$ intensity at −0.5 V is about 20 times smaller than that at +0.5 V. The difference is 29 times for −1.0 V and +1.0 V data (Fig. S5, supplementary material). Similar results are observed when measuring the STS at different tunneling-heights. Since the constant-height d$I$/d$V$ signal is determined by the LDOS of the surface and the tunneling matrix between the surface and tip, the above observations imply that there should be a big DOS difference between the occupied and unoccupied electronic states or a big tunneling matrix difference when tunneling happens from these states. From DFT results, we find comparable VB and CB LDOS, as shown in Fig. 2(b). Therefore, the large d$I$/d$V$ intensity difference observed in our experiments suggests a significant difference in the tunneling matrix. This is surprising since the tunneling matrix is normally assumed constant. As the tunneling matrix describes the overlap of wave functions of tip and sample, and the tip is unchanged during the measurement, we propose that the wave functions of CB's should extend more pronouncedly into the Z direction (inter-layer or tunneling direction) than those of VB's. This produces a larger tunneling matrix for the CB, and consequently the very high d$I$/d$V$ intensity in constant-height STS measurements. This also explains the significant tip-height change when the polarity of the bias is reversed in constant current scanning. The above discussion implies that the wave function distribution of the lowest CB is very special.

By taking the tunneling matrix into account, we re-examine the band structure of BP to understand why the STS spectrum is linear even when additional bands are involved in the energy region above 0.5 eV. In Fig. 2(a), we notice that in the energy range from the CBM to ∼1.41 eV, the CB is very steep in the Γ-Z direction, while the higher conduction bands are more "flat." This indicates that the states of the CB are more delocalized in the Z direction while the states of other bands are localized. By plotting the square of wave function distribution along Z direction for the VB, CB, CB + 1, CB + 2, and CB + 3 [shown in Fig. 3(a)], we see that there is a sharp contrast of the wave function of the CB compared with those of the VB and other higher energy unoccupied bands. The former decays imperceptibly in the BP interlayer and accordingly extends into the vacuum

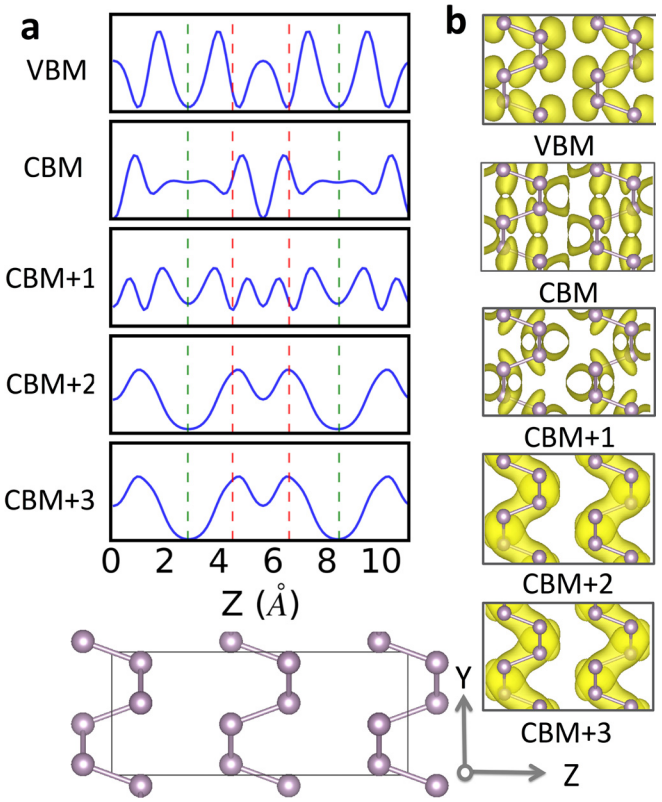


FIG. 3. (a) The corresponding atomic structure and the xy-averaged wave function square distribution of electronic states of highest VB, lowest CB, CB + 1, +2, +3 along Z direction. The red dash lines represent the atomic position of the center BP layer, and the green dash lines represent the center of the interlayer. (b) The corresponding spatial distributions of the orbitals.

significantly, while others decay very fast with limited density extending. Through plotting out wave function square around Γ point in these bands [Fig. 3(b)], we find that the CB is mainly composed of the $s$ and $P_z$ component, while the states of other bands are dominated by the $P_x$, $P_y$ components. It appears that it is the $P_z$ component that makes the states of the CB band significantly extended along $z$ direction. As a result, the tunneling matrix of CB is much bigger than other bands and the tunneling from CB dominates the STS signal, producing the experimentally observed linear STS spectra over the energy window from the CBM up to ∼1.41 eV. This delocalized wave function distribution of the CB along Z direction provides a unique opportunity for engineering electronic phase of BP, as a recent study implies, where BP is successfully transformed from a semiconductor to Dirac semimetal upon surface deposition of alkali metal atoms.[18]

## IV. CONCLUSION

In conclusion, we present the first observation of a robust, linear STM d$I$/d$V$ spectrum over a wide energy window in BP. By first principles calculations, analytic fitting, and model simulations, we demonstrated that the linear d$I$/d$V$ reveals two unique electronic characteristics of the CB in BP. First, the CB of BP exhibits highly anisotropic characteristics. In the quasi "3D" BP, this specific band anisotropy with one linear band along Γ-Y combined with two quadratic

bands along Γ-X and Γ-Z results in a strict linear DOS in the energy range just above CBM. This conclusion might be applicable to other material systems, which have similar layered structure and anisotropic bands as BP. Second, we conclude that the wave function of the CB extends into the BP interlayer and vacuum appreciably compared with those of adjacent bands, resulting into the monotonous linear STS profile up to high energy range. This property endows the CB an important role in tuning the electronic structures of the BP based materials upon external modulations. Our findings of the unique band features of the CB of BP provides insights into the fundamentals of the electronic structure of BP, as well as offering additional opportunities to engineer the electronic and optical properties of similar materials.

## SUPPLEMENTARY MATERIAL

See supplementary material for the methods used to measure the bandgaps and checking the validity of the band dispersion fitting.

## ACKNOWLEDGMENTS

The authors thank Professor Hrvoje Petek for fruitful discussions. This work is supported by the Natural Science Foundation of China (Project Nos. 11574364 and 11774267). M.F. acknowledges the support from the Thousand Talents Plan Program for Young Scientists and the Faculty Research Initiative Fund from School of Physics and Technology of Wuhan University. We thank the Supercomputer Center of Wuhan University and Environmental Molecular Sciences Laboratory at the PNNL, a user facility sponsored by the DOE Office of Biological and Environmental Research for providing calculation resources.

[1]L. Li, Y. Yu, G. J. Ye, Q. Ge, X. Ou, H. Wu, D. Feng, X. H. Chen, and Y. Zhang, Nat. Nanotechnol. **9**, 372 (2014).
[2]H. Liu, A. Neal, Z. Zhu, Z. Luo, X. Xu, D. Tomanek, and P. Ye, ACS Nano **8**, 4033 (2014).
[3]F. Xia, H. Wang, and Y. Jia, Nat. Commun. **5**, 4458 (2014).
[4]A. Castellanos-Gomez, J. Phys. Chem. Lett. **6**, 4280 (2015).
[5]X. Ling, H. Wang, S. Huang, F. Xia, and M. Dresselhaus, Proc. Natl. Acad. Sci. U. S. A. **112**, 4523 (2015).
[6]H. Liu, Y. Du, Y. Deng, and P. Ye, Chem. Soc. Rev. **44**, 2732 (2015).
[7]B. C. Yang, B. S. Wan, Q. H. Zhou, Y. Wang, W. T. Hu, W. M. Lv, Q. Chen, Z. M. Zeng, F. S. Wen, J. Y. Xiang, S. J. Yuan, J. L. Wang, B. S. Zhang, W. H. Wang, J. Y. Zhang, B. Xu, Z. S. Zhao, Y. J. Tian, and Z. Y. Liu, Adv. Mater. **28**, 9408 (2016).
[8]Z. N. Guo, S. Chen, Z. Z. Wang, Z. Y. Yang, F. Liu, Y. H. Xu, J. H. Wang, Y. Yi, H. Zhang, L. Liao, P. K. Chu, and X. F. Yu, Adv. Mater. **29**, 1703811 (2017).
[9]T. Hong, B. Chamlagain, W. Lin, H.-J. Chuang, M. H. Pan, Z. X. Zhou, and Y.-Q. Xu, Nanoscale. **6**, 8978 (2014).
[10]R. Keyes, Phys. Rev. **92**, 580 (1953).
[11]D. M. Warschauer, J. Appl. Phys. **34**, 1853 (1963).
[12]Y. Akahama, S. Endo, and S. Narita, J. Phys. Soc. J. **52**, 2148 (1983).
[13]A. S. Rodin, A. R. Carvalho, and A. H. C. Neto, Phys. Rev. Lett. **112**, 176801 (2014).
[14]J. Qiao, X. Kong, Z.-X. Hu, F. Yang, and W. Ji, Nat. Commun. **5**, 4475 (2014).
[15]R. Fei and L. Yang, Nano Lett. **14**, 2884–2889 (2014).
[16]G. Q. Huang, Z. W. Xing, and D. Y. Xing, Appl. Phys. Lett. **106**, 113107 (2015).
[17]J. Guan, Z. Zhu, and D. Tomanek, Phys. Rev. Lett. **113**, 046804 (2014).
[18]J. Kim, S. Baik, S. Ryu, Y. Sohn, S. Park, B. Park, J. Denlinger, Y. Yi, H. Choi, and K. Kim, Science **349**, 723–726 (2015).
[19]C. D. Zhang, J. C. Lian, W. Yi, Y. H. Jiang, L. W. Liu, H. Hu, W. D. Xiao, S. X. Du, L. L. Sun, and H. J. Gao, J. Phys. Chem. C **113**, 18823 (2009).
[20]B. Kiraly, N. Hauptmann, A. Rudenko, M. I. Katsnelson, and A. A. Khajetoorians, Nano Lett. **17**, 3607 (2017).
[21]Z. Qiu, H. Fang, A. Carvalho, A. S. Rodin, Y. Liu, S. Tan, M. Telychko, P. Lv, J. Su, Y. Wang, A. H. Castro Neto, and J. Lu, Nano Lett. **17**, 6935 (2017).
[22]J. V. Riffle, C. Flynn, B. St. Laurent, C. A. Ayotte, C. A. Caputo, and S. M. Hollen, J. Appl. Phys. **123**, 044301 (2018).
[23]L. B. Liang, J. Wang, B. G. Sumpter, V. Meunier, and M. H. Pan, Nano Lett. **14**, 6400 (2014).
[24]S. Marchini, S. Günther, and J. Wintterlin, Phys. Rev. B **76**, 075429 (2007).
[25]G. Li, A. Luican, and E. Y. Andrei, Phys. Rev. Lett. **102**, 176804 (2009).
[26]K. S. Novoselov, A. K. Geim, S. Morozov, D. Jiang, M. Katsnelson, I. Grigorieva, S. Dubonos, and A. A. Firsov, Nature **438**, 197 (2005).
[27]A. C. Neto, F. Guinea, N. M. Peres, K. S. Novoselov, and A. K. Geim, Rev. Mod. Phys. **81**, 109 (2009).
[28]Z. Qin, J. Pan, S. Lu, Y. Shao, Y. Wang, S. Du, H. J. Gao, and G. Cao, Adv. Mater. **29**, 1606046 (2017).
[29]L. Zhang, P. Bampoulis, A. Rudenko, Q. Yao, A. Van Houselt, B. Poelsema, M. Katsnelson, and H. Zandvliet, Phys. Rev. Lett. **116**, 256804 (2016).
[30]G. Kresse and J. Furthmuller, Phys. Rev. B **54**, 11169 (1996).
[31]G. Kresse and J. Furthmuller, Comput. Mater. Sci. **6**, 15 (1996).
[32]J. P. Perdew, K. Burke, and M. Ernzerhof, Phys. Rev. Lett. **77**, 3865 (1996).
[33]P. E. Blochl, Phys. Rev. B **50**, 17953 (1994).
[34]G. Kresse and D. Joubert, Phys. Rev. B **59**, 1758 (1999).
[35]J. Klimes, D. R. Bowler, and A. Michaelides, Phys. Rev. B **83**, 195131 (2011).
[36]J. Klimes, D. R. Bowler, and A. Michaelides, J. Phys. Condens. Matter **22**, 022201 (2010).
[37]A. Brown and S. Rundqvist, Acta Cryst. **19**, 684 (1965).
[38]N. D. Lang, Phys. Rev. B **34**, 5947 (1986).
[39]T. Vy, R. Soklaski, Y. Liang, and L. Yang, Phys. Rev. B **89**, 235319 (2014).
[40]X. Wang, A. M. Jones, K. L. Seyler, V. Tran, Y. Jia, H. Zhao, H. Wang, L. Yang, X. Xu, and F. Xia, Nat. Nanotechnol. **10**, 517 (2015).
[41]N. Mao, J. Tang, L. Xie, J. Wu, B. Han, J. Lin, S. Deng, W. Ji, H. Xu, K. Liu, L. Tong, and J. Zhang, J. Am. Chem. Soc. **138**, 300 (2016).
[42]J. Tao, W. Shen, S. Wu, L. Liu, Z. Feng, C. Wang, C. Hu, P. Yao, H. Zhang, W. Pang, X. Duan, J. Liu, C. Zhou, and D. Zhang, ACS Nano **9**, 11362 (2015).